Chapter 3

Mn-Bi alloys

Chapter 3: MnBi alloys

3.1. Introduction

In this chapter, the effect of room temperature high-energy ball milling on the magnetic properties of LTP MnBi has been studied. Ball milling was employed to reduce the particle size of the phase of interest as it enhances the coercivity values. Since the LTP is a line compound and there is Mn evaporation during the planned vacuum-arc melting route, the effect of ball milling was studied with varying Mn concentration. The $Mn_{55+x}Bi_{45-x}$ (x = 0, 1, 3, 5, 8) alloys were prepared from vacuum arc melting and subjected to a homogenization treatment. Consequently, these were manually crushed before subjecting to ball milling for 8 h. The sample was collected even after 4 h interval of milling. The initially as-cast and homogenized samples were also characterized with the help of XRD, SEM and DSC. The milled samples were further analysed under XPS, MPMPS, XRD, SEM and TEM for their morphological, structural and magnetic properties. In this work, unprecedented room temperature spontaneous exchange bias (SEB) in Mn-Bi high-energy ball milled powders was observed. As SEB increases the coercivity and thereby their $(BH)_{max}$ in permanent magnets, the possible physical mechanism of associated SEB effect in such inhomogeneous systems is also discussed.

3.2. Results and Discussion:

Figure 3.1(a-c) represent the XRD patterns of $Mn_{55+x}Bi_{45-x}$ (x = 0, 1, 3, 5, 8) alloys after arc melting and homogenizing as well as after ball milling for 4 and 8 h. Evidently, the diffraction patterns (Fig. 3.1a) point to the existence of three phases i.e., Bi, Mn and the

desired LTP MnBi phase. Although annealing at 573 K for 24 h promotes the formation of LTP MnBi, it does not produce a single phase of LTP MnBi (Fig. 3.1a) [1][2].

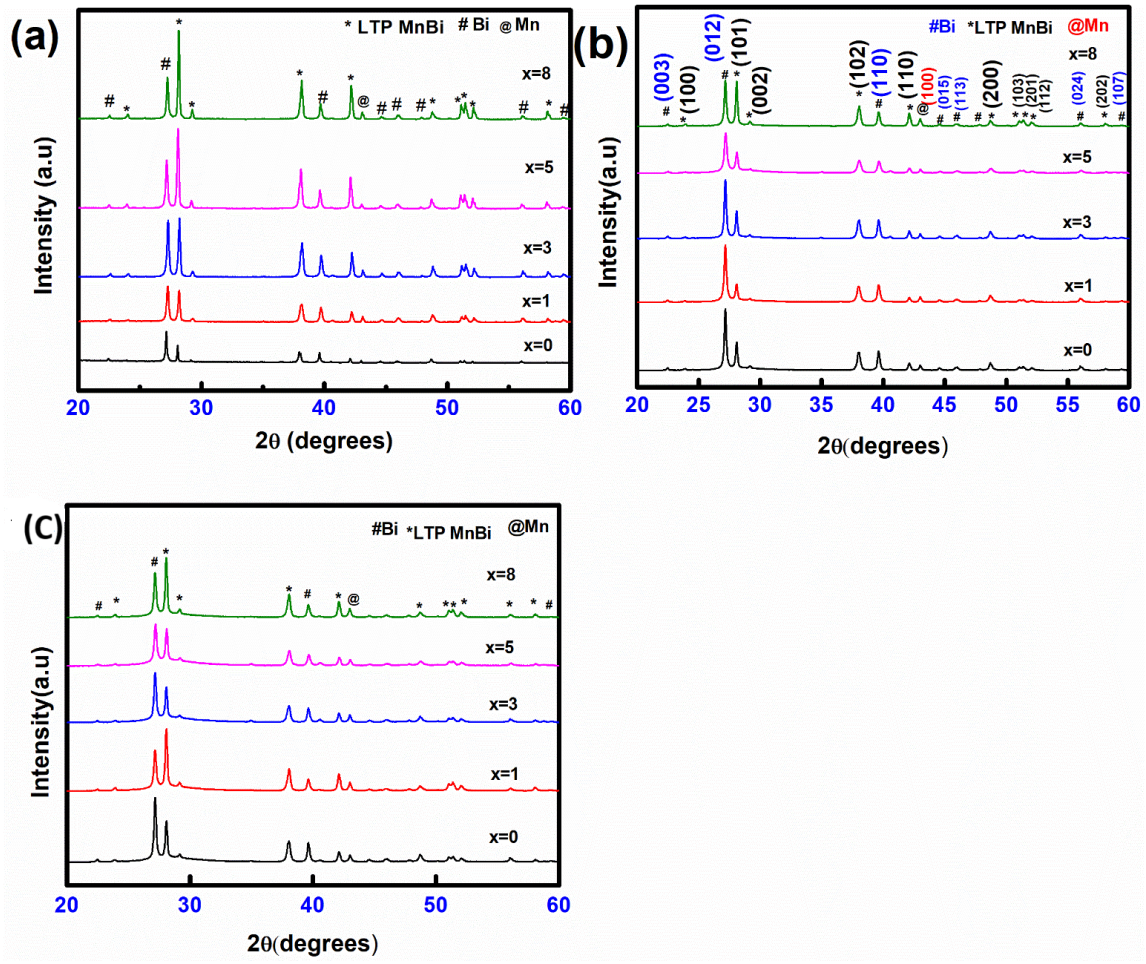

Figure 3.1. XRD patterns of (a) arc-melted and homogenized, (b) after 4 h and (c) after 8 h milled $Mn_{55+x}Bi_{45-x}$ (x = 0, 1, 3, 5, 8) alloys.

This is because, the line compound LTP MnBi forms through a peritectic reaction from the Mn-Bi liquid (~ 628 K). The single-phase formation is hampered by the segregation and sluggish diffusion of Mn from the liquid. In addition, arc melting process does not provide sufficient cooling rate to prevent the precipitation of Mn from the melt [2]. With enhanced Mn content, the volume fraction of MnBi phase was also found to be increasing as

shown in the Fig. 3.1 (a). Further, with the improved concentration of Mn, the Bi phase was seemed to be reducing. The phase diagram suggests that increasing Mn content in the initial Mn–Bi composition (before solidification) increases the amount of Mn precipitate and reduces the Bi rich liquid which eventually results in smaller Bi content [3].

Ball milling for these samples was done to achieve finer grain microstructure to enhance the coercivity [4]. The XRD patterns of ball milled samples showed broadening of peaks in comparison to the homogenized samples, suggesting a reduction in grain size (Figure 1 b and c). After 4 h of milling, the concentration of MnBi was reduced for all the samples indicating the decomposition of MnBi phase into Mn and Bi (Figure 3.1b). However, the content of MnBi mildly increased after 8 h, which might be due to mechanical alloying between unreacted Mn and Bi during milling for extended duration (Figure 3.1c). The decrease in the relative peak intensity of MnBi and the increase in the peak intensities of Bi and Mn corroborates its decomposition (Figure 3.1b). The increase in the mechanical strain with milling time is supposed to be the cause of decomposition of the phase (Figure 3.2). This observation is consistent with previously published results by Yin et al. which suggests that milling causes defects and disorder in the system [5].The average crystallite size was calculated from the peak widths using Williamson-Hall plot after considering the instrumental broadening. The average crystallite size of the homogenised as well as 4 and 8 h milled samples was calculated to be 220, 89, and 58 nm respectively. The crystallite size of LTP MnBi phase decreased with milling time as shown in Figure 3.2.

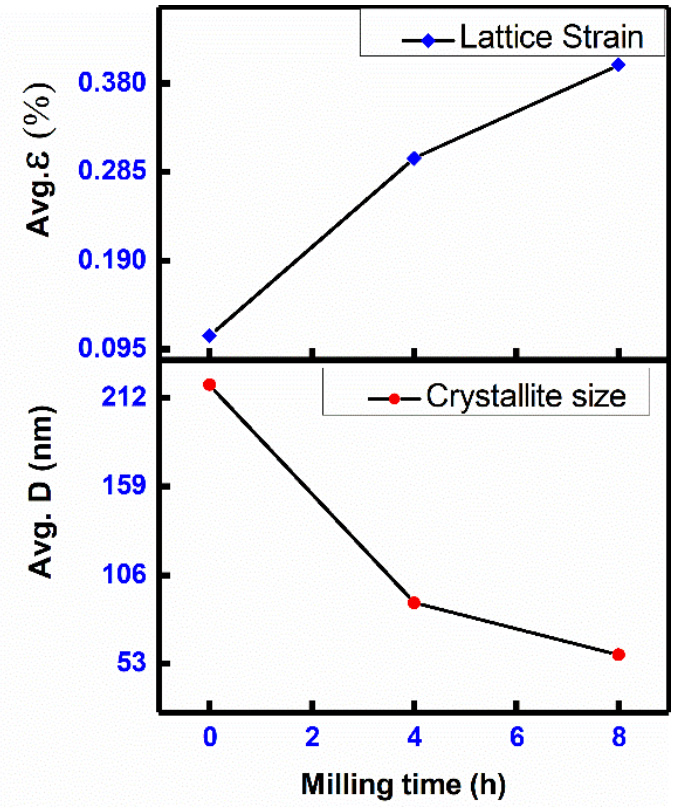

Figure 3.2. Variation of average crystallite size and average lattice strain with milling time.

Thermal Analysis:

The DSC curve of $Mn_{55}Bi_{45}$ homogenized sample obtained at a moderate heating rate of 10 °C/min under flowing N_2 gas also advocate for the formation of the LTP MnBi (Fig. 3.3). The sharp endothermic peaks in the curve indicate the structural changes in the sample with increasing temperature. The endothermic peak at 267.2 °C (represented by point A) indicates the characteristic melting temperature of the Bi-rich eutectic phase [6]. The LTP-HTP (high temperature phase) transition is evidenced from the peak at 362.6 °C (point B). The sharpest endothermic peak at B proved the large content of LTP MnBi. This endothermic peak represents the energy change that occurred at the curie temperature of LTP MnBi due to

ferromagnetic to paramagnetic transition [7]. The third endothermic peak (C) at 455.4 °C corresponds to the peritectic decomposition of the HTP MnBi phase [8].

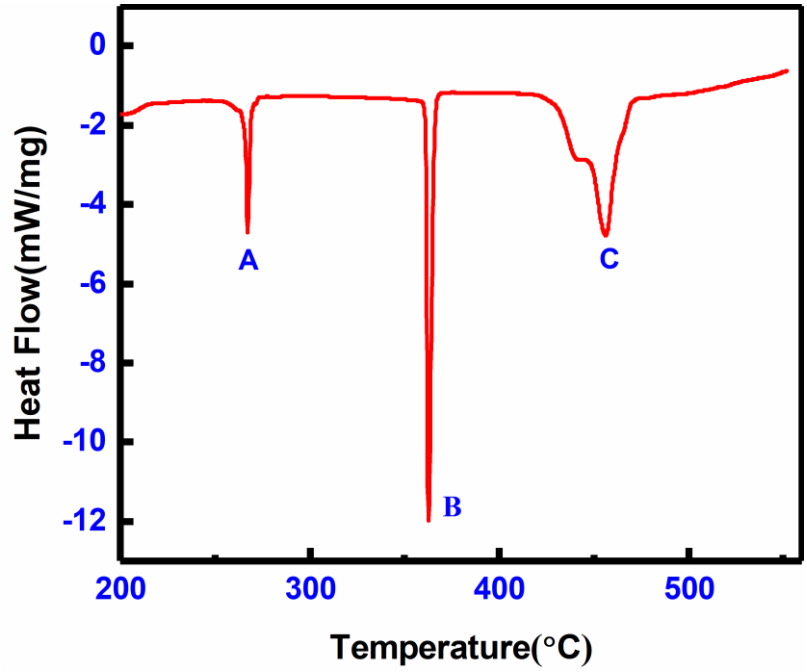

Figure 3.3. DSC curve of arc-melted and homogenised $Mn_{55}Bi_{45}$ alloy.

SEM Analysis:

To further investigate the particle size distribution and surface morphology, SEM images of the as cast and ball milled powders were taken and given in Fig. 4. The Fig. 4 a shows Mn, Bi and MnBi particles which were identified with the help of EDS. Insets of figure 4b and 4c depict the particle size distribution after 4 and 8 h of milling. The particle size distribution analysis was done with the help of Image J software.

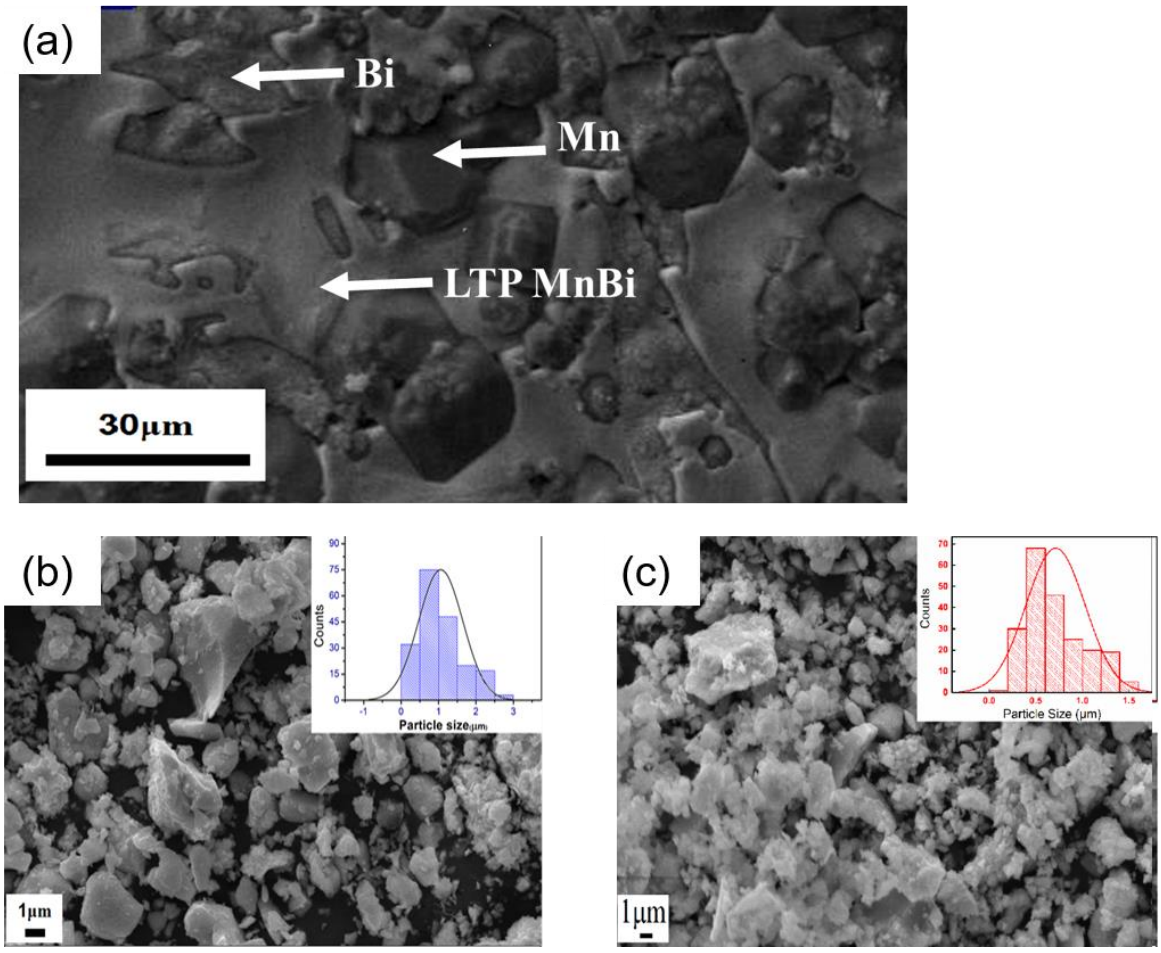

Figure 3.4. SEM micrographs of (a) homogenized $Mn_{55}Bi_{45}$ alloy, (b) after 4 h and (c) after 8 h of milling (insets depict the respective particle size distribution after milling).

The SEM image of the homogenized alloy ($Mn_{55}Bi_{45}$) (Fig. 3.4 a) showed embedded Mn metal in the LTP MnBi, implying its formation is due to transformation of HTP to LTP. The HTP (~ 54.3 at% Mn), transforms to LTP (~ 50 at% Mn) and Mn between 340 and 355 ºC [9]. Cui et al. identified the ideal composition for MnBi alloy containing maximum LTP MnBi phase, resulting in largest saturation magnetization (M_S) at room temperature to be 55 at % Mn [2]. The Mn-Bi alloys with compositions >55 at% Mn, in the aforesaid temperature

range, generally contain Mn, HTP MnBi, and a liquid Bi-rich phase. Further, HTP MnBi transforms to the LTP MnBi and Mn phase at lower temperatures. Simultaneously, the liquid Bi-rich phase transforms into the LTP MnBi and a liquid phase with more Bi, finally decomposing to the LTP MnBi and Bi. Because the initial composition is to the right of the HTP composition, it resulted in the formation of a smaller volume of the liquid Bi-rich phase. Thus, the final Bi phase is minor. The XRD patterns of Fig. 3.1 (a) were in accordance with this solidification sequence.

Further, it was observed that with milling, the coarse and irregular pieces reduced down to smaller polycrystalline particles. The mean particle size reduced to 0.85 ± 0.13 μm and 0.56 ± 0.17μm after 4 and 8 h of milling respectively as shown in the insets of Fig 3.4(b) and (c). The refined LTP MnBi polycrystalline particles with a narrow size distribution were obtained as the collision energy between the grinding balls has been effectively transferred to the powder samples during the high-energy ball milling process. In spite of performing the ball milling in toluene environment, certain extent of oxidation was seen from the EDS of the milled sample; which is unavoidable for extremely fine particles [10,11]

TEM Analysis:

TEM was utilized to further examine the effects of the high-energy ball-milling process at nano level, on the microstructure of the MnBi particles. The microstructure of 8 h ball milled $Mn_{55}Bi_{45}$ alloy powder, as bright field image and resulting selected area diffraction (SAD) pattern are shown in Fig. 3.5. In the bright field image, grains that are elongated and agglomerated with flaky morphology are observed. The presence of spot pattern in the SAD pattern indicates the presence of all the three phases.

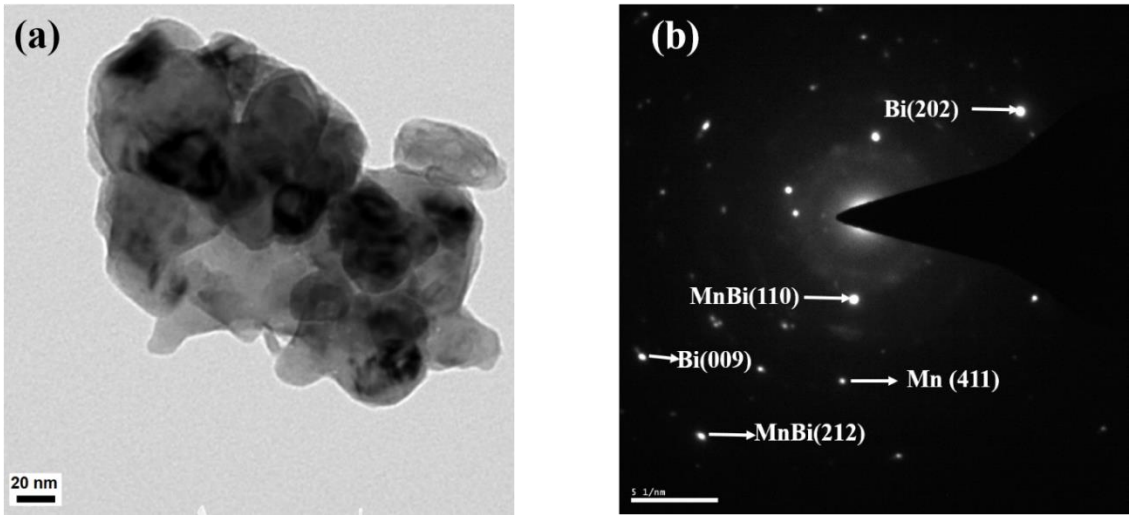

Figure 3.5. (a) Bright Field TEM image of $Mn_{55}Bi_{45}$ alloy after 8 h of milling and (b) corresponding diffraction pattern showing the LTP MnBi phase.

XPS Analysis:

X-ray photoelectron spectroscopy (XPS), was carried out to observe the oxidation states of the elements in $Mn_{55}Bi_{45}$ sample obtained after 8 h of milling. Figure 3.6 displays the high-resolution XPS spectrum of Mn2p, Bi 4f and O 1s. The Mn 2p XPS spectrum (Fig 6a) was splitted into two peaks, Mn 2p3/2 at 642.89 and Mn 2p1/2 state at 654.71 eV, due to spin-orbit coupling. Further, the spectrum was de-convoluted with nine peaks considering Shirley background, using standard XPS software. The peaks at 638.65(650.95) eV,641.10(652.81) eV, 642.39(654.45) eV, 643.48(655.95) eV, were due to Mn(0), Mn2+, Mn3+ and Mn4+ states respectively. In addition, a satellite peak corresponding to MnO was observed at 644.67 eV [12]. The presence of multivalent oxidation states suggest that oxidation might have occurred on the surface of ball-milled powders. The Bi 4f XPS spectrum profile (Fig 3.6b), comprising of two strong peaks at around 159.62 eV and 164.94

eV was the characteristic energy band for Bi 4f 7/2 and 4f 5/2, respectively. The Bi 4f 7/2 and 5/2 envelopes was de-convoluted to Bi metal (158.61 eV and 163.96 eV) and Bi_2O_3 (157.66 and 163.1 eV) [13]. The peaks seen at 529.8 and 532.2 eV for O 1s profile (Fig 6c) can be attributed to the oxygen ions (O_2^-) and oxygen species adsorbed on the sample surface respectively[14].

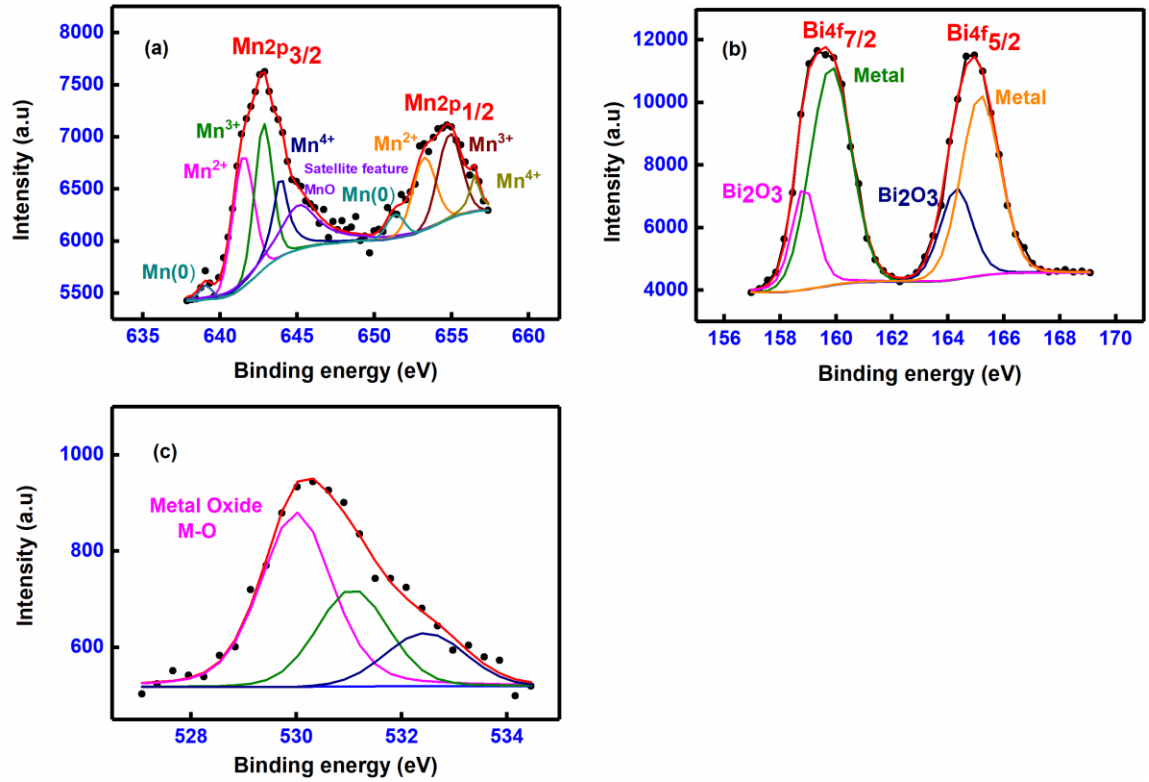

Figure 3.6. XPS survey spectra for (a) Mn 2p (b) Bi 4f and (c) O 1s for 8 h ball milled $Mn_{55}Bi_{45}$ sample.

Magnetic behaviour Analysis:

The room temperature hysteresis loops (M-H) of the 4 and 8 h ball milled samples are presented in figure 7. The obtained hysteresis loops displayed a kink. This may be due to different coercivities arising from the inhomogeneous particle size distribution [15].

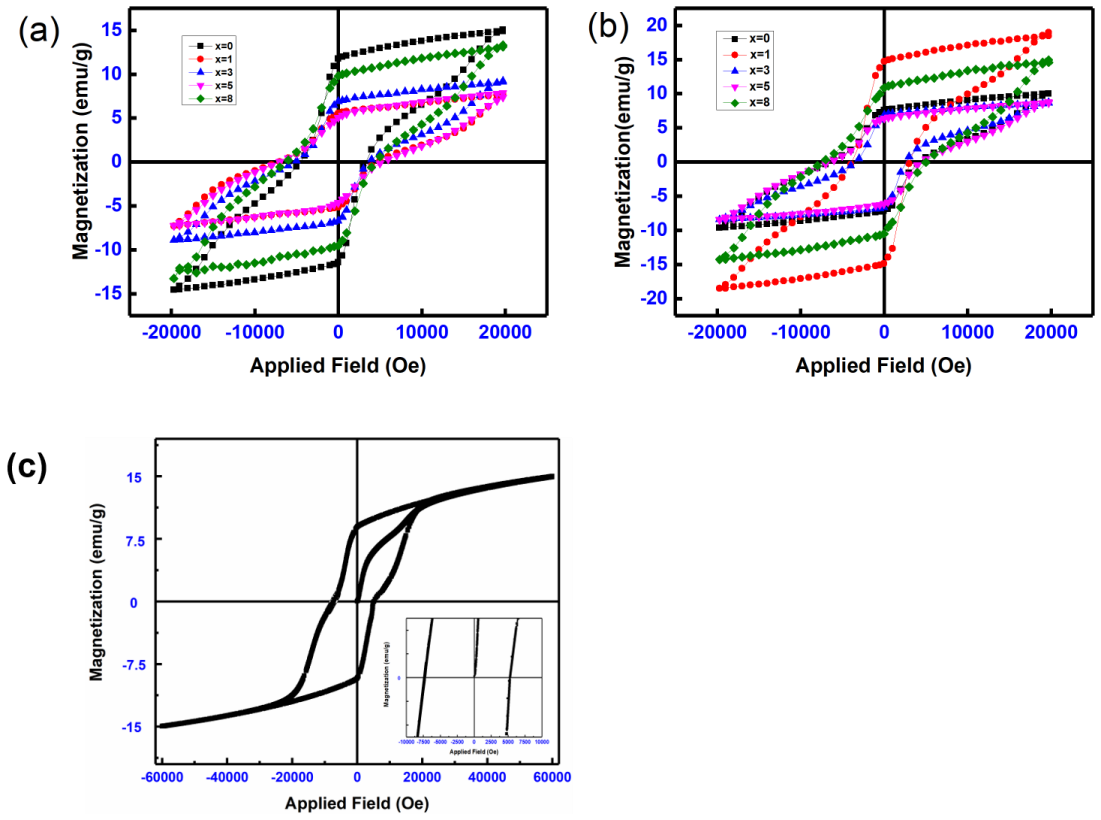

Figure 3.7. Room temperature M *vs.* H curves (a) after 4 h (b) after 8 h of milling of $Mn_{55+x}Bi_{45-x}$ (x = 0, 1, 3, 5, 8) alloys and (c) x=8 after 8 h of milling at 60 kOe field. Insets show the shift in the loops along the horizontal axis.

In accordance to the decrease of crystallite size, the microstructure sensitive coercive force H_C was improved with milling period. It reaches a maximum value of 7.4 kOe upon 8 h of milling for x = 8 sample. As reported in many hard magnetic materials, improvement

of H_C is also owing to the reduction in particle size [16][17]. Another contributing factor is the decomposition of LTP MnBi with milling, which creates non-ferromagnetic phases (Bi and Mn). This decomposition positively affects the coercivity by separating the magnetic grains of ferromagnetic MnBi [10]. The variation of coercivity with Mn addition for 4 and 8 h milled samples is shown in Figure 3.8.

During ball milling process, two competing mechanisms are supposed to be taking place i.e., fracturing of particles into finer size and cold welding of particles. In case of MnBi, apart from the decomposition of LTP MnBi phase with high energy milling, the unreacted Mn and Bi also mechanically alloyed to form MnBi. These two competing processes are proposed to be the cause for non-regular decomposition trend in 8 h milled samples. Variation of M_S and M_r can be seen for 4 and 8 h milled samples in Figure 3.8. The optimum M_S value after 4 and 8 h of milling was around 14.35 and 19 emu/g respectively. Though, the obtained values are much lower than the calculated theoretical M_S value (~ 81 emu/g) for LTP MnBi but are comparable with some of the reported data [10,18].

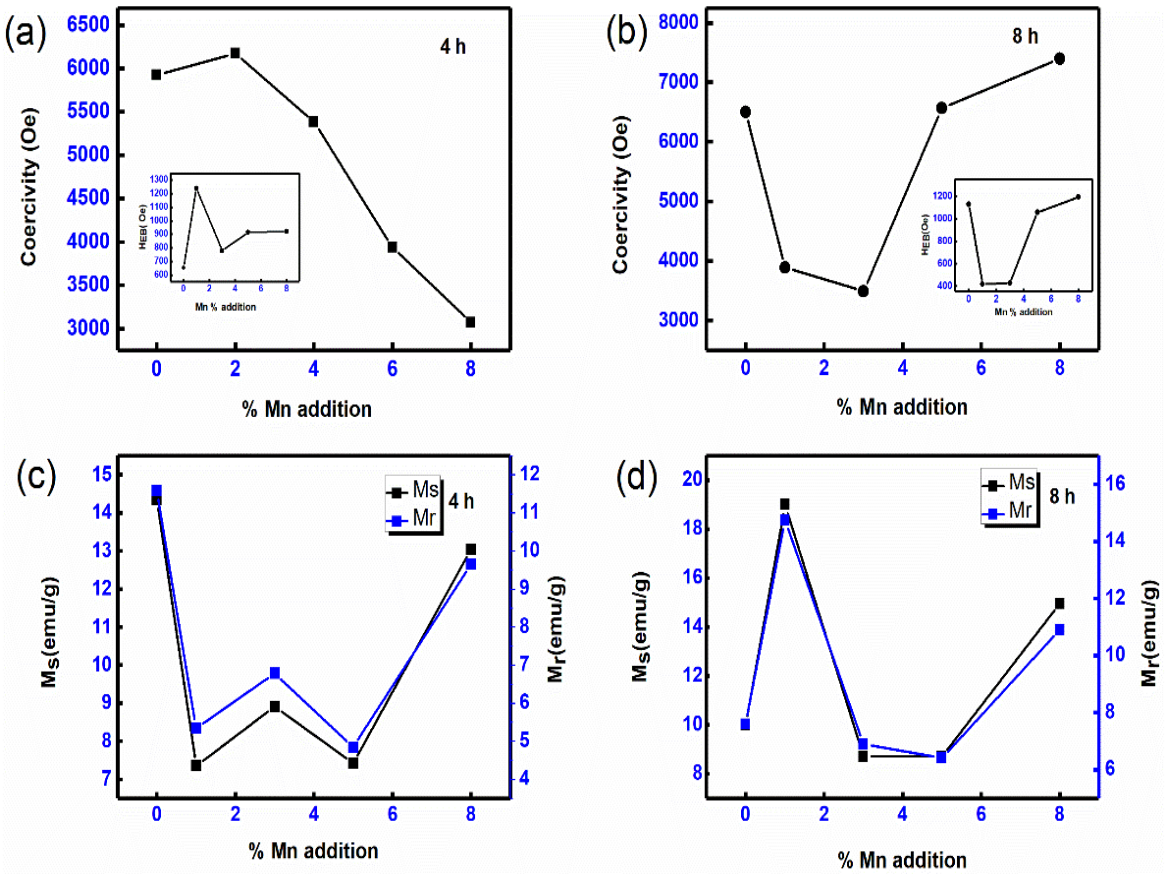

Figure 3.8. Variation of coercivity values with % Mn addition after (a) 4 h, (b) 8 h milling, and variation of M_S and M_r values with % Mn addition after (c) 4 h, (d) 8 h milling for $Mn_{55+x}Bi_{45-x}$ (x = 0, 1, 3, 5, 8) alloys at 2T applied field. Insets of (a) and (b) show the variation of H_{EB} with %Mn addition for 4 and 8 h of milling, respectively.

It could be understood that in the unit cell of LTP MnBi, two Mn atoms occupy (0, 0, 0) and (0, 0, 1/2) -octahedral 2a sites and two Bi atoms fill the (1/3, 2/3, 1/4) and (2/3, 1/3, 3/4) - 2c sites. Reports show that milling causes the residing site transition of Mn atoms from sites of the original Mn lattice to the interstitial Bi equivalent sites giving rise to anti-site disorders [19][20].The HTP to LTP transformation at 340 ºC is associated with the diffusion of Mn into the interstitial void of LTP MnBi unit cell reducing Mn-Mn distance. This way

the interstitial Mn couples antiferromagnetically with the octahedral 2a site Mn resulting in lower M_S value [21]. The decrease of M_S value could also be due to the reduction in weight proportion of ferromagnetic MnBi phase which decomposes during the milling process into elemental form [15]. The XRD results, as shown above, evidenced the decrease of weight proportion of MnBi phase (Figure 3.1 b). Together, XRD and magnetization behaviour validate the decomposition of MnBi phase during milling. Along with MnBi decomposition , the oxidation of surface of MnBi particles cause the saturation magnetization (an atomic order arranging indicator) to decrease, which shows the disordering of atomic configuration.

Intriguing as shown in the insets of Fig. 3.7 spontaneous exchange bias was observed by the shift in the hysteresis loop along the horizontal axis. If H_R and H_L are right and left coercivities respectively, the exchange bias field (H_{EB}) can be quantified by the formula $H_{EB} = (H_L + H_R)/2$. A maximum spontaneous H_{EB} achieved was around 1200 Oe at room temperature for x =8 sample after 8 h of milling (Figure 3.7 b). The H_{EB} indicates strength of exchange coupling between the FM and the AFM components. So far, such phenomenon has not been reported for MnBi particles in the literature. In the earlier studies, the samples were magnetically field separated or pressed before the measurement, showing no exchange bias effect [22]. In this study, the large H_{EB}, greater than that observed in Heusler alloys, can be ascribed to the improvement of AFM interactions and thereby facilitating the pinning of the FM region domains by the AFM region. Further, to verify that the observed exchange bias was not due to lack of saturation at the applied field (i.e. 2 T), hysteresis loop was taken for the same sample up to 6 T (Figure 3.7 c). At this field also, the sample exhibited equal values

of M_S and H_{EB} (~1200 Oe). This negated the possibility of minor loop effects in the present samples.

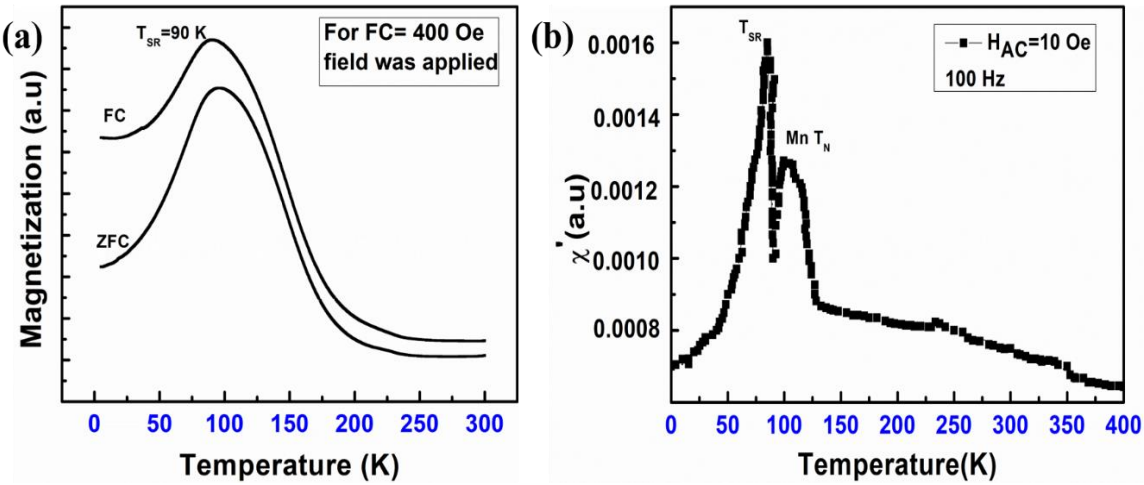

Figure 3.9. (a) Zero Field cooled (ZFC) and Field cooled (FC) curves and (b) AC susceptibility measurements of x=8 sample after 8 h of milling.

To corroborate the formation of AFM interactions ZFC and FC magnetic measurements were taken from 5 K to 300 K for the sample with highest H_{EB}. In the case of FC curves, a nominal field of 400 Oe was applied. As shown in Figure 3.9a, a single peak has been observed corresponding to the spin reorientation temperature of LTP MnBi. With decreasing temperature, MnBi exhibits a spin reorientation transition at 90 K (T_{SR}), below which the magnetic moment lies in the ab-plane. Above T_{SR}, the magnetic anisotropy increases up to the decomposition temperature near 630 K [23]. Apart from T_{SR}, no other peaks were observed suggesting the absence of any magnetic phases apart from LTP. The divergence between the ZFC and FC curves suggest that the sample is compositionally uniform but magnetically inhomogeneous. To further study the inhomogeneity, AC susceptibility measurements were again conducted below the room temperature up to 5 K.

This study as can be seen in figure 3.9b, performed at a frequency of 100 Hz and 10 Oe A.C field, showed two peaks at 90 K and 100 K, respectively. The 90 K peak corresponds to the T_{SR} where as the 100 K peak refers to the local AFM clusters of Mn since the neel temperature of AFM Mn is around 100 K [24].

The presence of SEB suggests local AFM clusters in an FM background leading to magnetically inhomogeneous states in the system. The LTP MnBi unit cell ($a = b = 4.290$ Å, $c = 6.126$ Å, $\alpha = \beta = 90$, $\gamma = 120$,) has large trigonal-bipyramidal interstitial vacancy sites, which Mn atoms or any other dopant can occupy [25]. Mn-Mn atomic distance strongly influences their spin ordering to be aligned parallel or anti-parallel. Reported studies in other magnetic alloys suggest Mn-Mn nearest neighbours with anti-parallel alignment of spin (AFM coupling) is favoured under higher content of Mn atoms. At the same time, a lower Mn concentration promotes enhanced FM coupling between next-nearest atomic neighbours giving rise to a local net magnetization [26].

A complex magnetic structure in MnBi results when Mn atoms occupy the large interstitial sites of the unit cell. Earlier reported studies speculated that ferromagnetically coupled Mn atoms occupy octahedral sites with their spin parallel to the c-axis. Also, the antiferromagnetic interaction between bipyramidal Mn atoms and the octahedral Mn atoms results in reduced net magnetization. For the reason that, the Mn-Mn inter atomic distance amid interstitial Mn atoms would possibly fall in an anti-ferromagnetic regime[27,28]. In addition; like Mn-rich Heusler alloys, it also exhibits anti-site disorder [29,30]. As this defect modulates the spin polarization, it results in a complex magnetic ground state by inducing competing magnetic interactions. It is proposed that factors like interstitial Mn atoms, anti-site disorders, and localized concentration fluctuations in the alloys lead to the formation of

AFM clusters during the synthesis of ball-milled MnBi powders. A model of spin scheme representing the magnetic configuration in the MnBi ball-milled powders is proposed in Figure 3.10 to visibly comprehend the mechanism of the exchange bias effect.

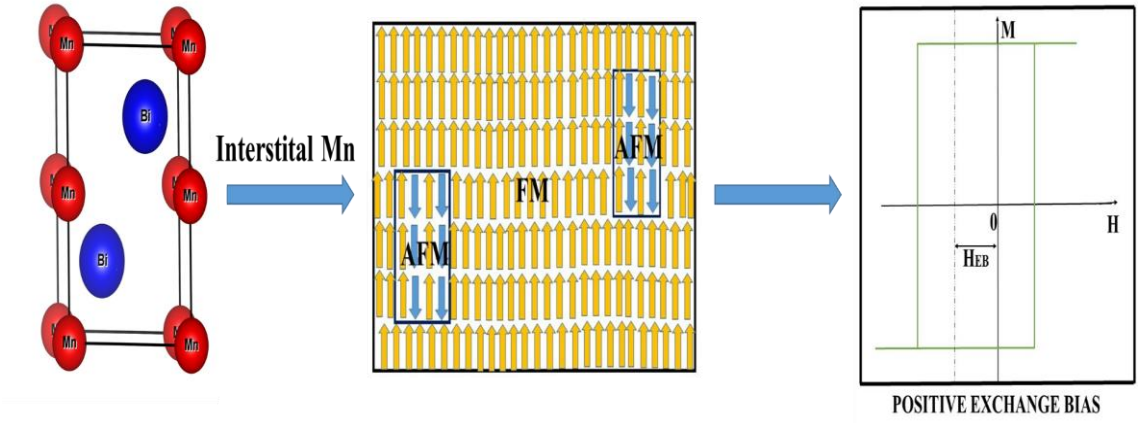

Figure 3.10. Pictorial representation of the proposed spin model for the presence of spontaneous exchange bias in ball milled $Mn_{55+x}Bi_{45-x}$ (x = 0, 1, 3, 5, 8) powders at room temperature.

The model assumes a single crystal of MnBi grain consisting of homogeneous AFM clusters in a homogeneous FM matrix. As discussed above, due to its composition and magnetic environment changes, the spin moment of the Mn atom reverses in the anti-parallel direction resulting in localized AFM clusters in the FM matrix. Under the application of an external magnetic field, the initial (virgin) magnetization process will tend to align the spin moments in the FM matrix and AFM clusters in the direction of the applied field. To minimize the energy, the spins at the interfaces of the FM and AFM phases will also align in the external field direction. This initiates the exchange interaction amidst the AFM clusters and the FM matrix in the MnBi alloy, which could account for the considerably large values

of H_{EB}. Such localized AFM clusters located inside the FM matrix and magnetically coupled to the matrix suffice for a possible explanation of spontaneous exchange bias in our system. This explanation is similar to the models explained by Kouvel et al. for Mn-Al system [29]. In conclusion, we have observed spontaneous exchange bias in MnBi high-energy ball milled powders, which can be utilized to enhance the energy product of the system by increasing the coercivity. A maximum spontaneous H_{EB} of 1200 Oe was observed at room temperature possibly due to the presence of AFM clusters in an FM matrix. In addition, this phenomenon in the alloy can be of interest due to its potential applications in spintronic devices.

3.3. Conclusions:

LTP MnBi phase was synthesized and confirmed by XRD and DSC. The H_C values increased with milling due to the reduction in particle size and the separation of magnetic MnBi with non-magnetic Bi and Mn. M_S values decreased from the theoretical values due to AFM interactions, surface oxidation, and MnBi phase decomposition during milling. SEB phenomenon was observed for all the alloys obtained after milling which gave high values of H_{SEB} (~ 1.2 kOe) and H_c (~ 7.5 kOe). This paves the way for MnBi system for more advanced applications.

3.4. References

[1] J. Cui, J.-P. Choi, E. Polikarpov, M.E. Bowden, W. Xie, G. Li, Z. Nie, N. Zarkevich, M.J. Kramer, D. Johnson, Effect of composition and heat treatment on MnBi magnetic materials, Acta Mater. 79 (2014) 374–381.

[2] N.V.R. Rao, A.M. Gabay, G.C. Hadjipanayis, Anisotropic fully dense MnBi permanent magnet with high energy product and high coercivity at elevated temperatures, J. Phys. D. Appl. Phys. 46 (2013) 62001.

[3] H. Yoshida, T. Shima, T. Takahashi, H. Fujimori, Preparation of highly pure MnBi intermetallic compounds by arc-melting, Mater. Trans. JIM. 40 (1999) 455–458.

[4] W. Xie, E. Polikarpov, J.P. Choi, M.E. Bowden, K. Sun, J. Cui, Effect of ball milling and heat treatment process on MnBi powders magnetic properties, J. Alloys Compd. 680 (2016) 1–5. https://doi.org/10.1016/J.JALLCOM.2016.04.097.

[5] F. Yin, N. Gu, T. Shigematsu, N. Nakanishi, Sintering formation of low temperature phase MnBi and its disordering in mechanical milling, J. Mater. Sci. Technol. 12 (1996) 335–341.

[6] Y.B. Yang, X.G. Chen, S. Guo, A.R. Yan, Q.Z. Huang, M.M. Wu, D.F. Chen, Y.C. Yang, J.B. Yang, Temperature dependences of structure and coercivity for melt-spun MnBi compound, J. Magn. Magn. Mater. 330 (2013) 106–110.

[7] C.S. Lakshmi, R.W. Smith, Effect of rapid quenching on the magnetic and structural properties of Bi-MnBi composites, J. Mater. Sci. 25 (1990) 465–471.

[8] X. Guo, Z. Altounian, J.O. Ström-Olsen, Formation of MnBi ferromagnetic phases through crystallization of the amorphous phase, J. Appl. Phys. 69 (1991) 6067–6069.

[9] T.B. Massalski, J.L. Murray, L.H. Bennett, H. Baker, Binary Alloy Phase Diagrams

(American Society for Metals, Metals Park, Ohio, 1986), Vol. I. (2017) 1100.

[10] S. Kavita, V. V Ramakrishna, A. Srinivasan, R. Gopalan, Structural and magnetic properties of the low temperature phase MnBi with ball milling, Mater. Res. Express. 3 (2016) 56102.

[11] J. Cao, Y.L. Huang, Y.H. Hou, Z.Q. Shi, X.T. Yan, Z.C. Zhong, G.P. Wang, Microstructure and magnetic properties of MnBi alloys with high coercivity and significant anisotropy prepared by surfactant assisted ball milling, J. Magn. Magn. Mater. 473 (2019) 505–510. https://doi.org/10.1016/j.jmmm.2018.10.052.

[12] A.M.E. Raj, S.G. Victoria, V.B. Jothy, C. Ravidhas, J. Wollschläger, M. Suendorf, M. Neumann, M. Jayachandran, C. Sanjeeviraja, XRD and XPS characterization of mixed valence Mn3O4 hausmannite thin films prepared by chemical spray pyrolysis technique, Appl. Surf. Sci. 256 (2010) 2920–2926.

[13] V.S. Dharmadhikari, S.R. Sainkar, S. Badrinarayan, A. Goswami, Characterisation of thin films of bismuth oxide by X-ray photoelectron spectroscopy, J. Electron Spectros. Relat. Phenomena. 25 (1982) 181–189.

[14] S.K. Shaw, A. Gangwar, A. Sharma, S.K. Alla, S. Kavita, M. Vasundhara, S.S. Meena, P. Maiti, N.K. Prasad, Structural and magnetic properties of nanocrystalline equi-atomic spinel high-entropy oxide (AlCoFeMnNi) 3O4 synthesised by microwave assisted co-precipitation technique, J. Alloys Compd. 878 (2021) 160269.

[15] N.V.R. Rao, G.C. Hadjipanayis, Influence of jet milling process parameters on particle size, phase formation and magnetic properties of MnBi alloy, J. Alloys Compd. 629 (2015) 80–83.

[16] G.C. Hadjipanayis, Nanophase hard magnets, J. Magn. Magn. Mater. 200 (1999) 373–391. https://doi.org/10.1016/S0304-8853(99)00430-8.

[17] N.V.R. Rao, R. Gopalan, M.M. Raja, V. Chandrasekaran, D. Chakravarty, R. Sundaresan, R. Ranganathan, K. Hono, Structural and magnetic studies on spark plasma sintered SmCo5/Fe bulk nanocomposite magnets, J. Magn. Magn. Mater. 312 (2007) 252–257.

[18] W. Xie, E. Polikarpov, J.-P. Choi, M.E. Bowden, K. Sun, J. Cui, Effect of ball milling and heat treatment process on MnBi powders magnetic properties, J. Alloys Compd. 680 (2016) 1–5.

[19] M. Choi, Y.-K. Hong, H. Won, G.J. Mankey, C.-D. Yeo, W. Lee, M.-H. Jung, T. Lee, J.-K. Lee, Suppressing antiferromagnetic coupling in rare-earth free ferromagnetic MnBi-Cu permanent magnet, J. Appl. Phys. 129 (2021) 113902.

[20] R. Coehoorn, R.A. De Groot, The electronic structure of MnBi, J. Phys. F Met. Phys. 15 (1985) 2135.

[21] P.R. Bandaru, T.D. Sands, Y. Kubota, E.E. Marinero, Decoupling the structural and magnetic phase transformations in magneto-optic MnBi thin films by the partial substitution of Cr for Mn, Appl. Phys. Lett. 72 (1998) 2337–2339.

[22] J.B. Yang, W.B. Yelon, W.J. James, Q. Cai, M. Kornecki, S. Roy, N. Ali, P. L'Heritier, Crystal structure, magnetic properties and electronic structure of the MnBi intermetallic compound, J. Phys. Condens. Matter. 14 (2002) 6509–6519. https://doi.org/10.1088/0953-8984/14/25/318.

[23] V.P. Antropov, V.N. Antonov, L. V Bekenov, A. Kutepov, G. Kotliar, Magnetic anisotropic effects and electronic correlations in MnBi ferromagnet, Phys. Rev. B - Condens. Matter Mater. Phys. 90 (2014). https://doi.org/10.1103/PhysRevB.90.054404.

[24] P. Kharel, R. Skomski, P. Lukashev, R. Sabirianov, D.J. Sellmyer, Spin correlations

and Kondo effect in a strong ferromagnet, Phys. Rev. B. 84 (2011) 14431.

[25] J.A. Kurzman, A.J. Martinolich, J.R. Neilson, Influence of interstitial Mn on local structure and magnetism in Mn 1+ δ Sb, Phys. Rev. B. 92 (2015) 184414.

[26] Y. Song, Z. Xiang, T. Wang, J. Niu, K. Xia, W. Lu, H. Zhang, Y. Cao, S. Yoshimura, H. Saito, High temperature exchange bias effect in melt-spun $Mn_{55}Bi_{45}$alloys, Appl. Phys. Lett. 109 (2016) 112402.

[27] A.F. Andresen, W. Hälg, P. Fischer, E. Stoll, The magnetic and crystallographic properties of MnBi studied by neutron diffraction, Acta Chem. Scand. 21 (1967) 1543–1554.

[28] T. Graf, C. Felser, S.S.P. Parkin, Simple rules for the understanding of Heusler compounds, Prog. Solid State Chem. 39 (2011) 1–50.

[29] J.S. Kouvel, The ferromagnetic-antiferromagnetic properties of copper-manganese and silver-manganese alloys, J. Phys. Chem. Solids. 21 (1961) 57–70.

[30] Heikes, R.R., 1955. Magnetic transformation in MnBi. *Physical Review*, *99*(2), p.446.